Glycobiology, 2022, **32**, 6, 483–495
https://doi.org/10.1093/glycob/cwac010
Advance access publication date 10 March 2022
Original Article

Structural characterization of human milk oligosaccharides using ultrahigh performance liquid chromatography–helium charge transfer dissociation mass spectrometry

Praneeth M Mendis[1], Glen P Jackson[1,2,*]

[1]C. Eugene Bennett Department of Chemistry, West Virginia University, Morgantown, WV 26506-6121, USA, [2]Department of Forensic and Investigative Science, West Virginia University, Morgantown, WV 26506-6121, USA

*Corresponding author: Email: glen.jackson@mail.wvu.edu

The combination of helium charge transfer dissociation mass spectrometry (He–CTD–MS) with ultrahigh performance liquid chromatography (UHPLC) is presented for the analysis of a complex mixture of acidic and neutral human milk oligosaccharides (HMOs). The research focuses on the identification of the monosaccharide sequence, the branching patterns, the sialylation/fucosylation arrangements, and the differentiation of isomeric oligosaccharides in the mixture. Initial studies first optimized the conditions for the UHPLC separation and the He–CTD–MS conditions. Results demonstrate that He–CTD is compatible with UHPLC timescales and provides unambiguous glycosidic and cross-ring cleavages from both the reducing and the nonreducing ends, which is not typically possible using collision-induced dissociation. He–CTD produces informative fragments, including $^{0,3}A_n$ and $^{0,4}A_n$ ions, which have been observed with electron transfer dissociation, electron detachment dissociation, and ultraviolet photodissociation (UVPD) and are crucial for differentiating the α-2,3- versus α-2,6-linked sialic acid (Neu5Ac) residues present among sialyllacto-*N*-tetraose HMOs. In addition to the linkage positions, He–CTD is able to differentiate structural isomers for both sialyllacto-*N*-tetraoses and lacto-*N*-fucopentaoses structures by providing unique, unambiguous cross-ring cleavages of types $^{0,2}A_n$, $^{0,2}X_n$, and $^{1,5}A_n$ while preserving most of the labile Neu5Ac and fucose groups.

Key words: branching position; fucosylation; linkage position; sialylation; structural characterization.

Introduction

Human breast milk is nature's gold standard of nutrition for newborns (Remoroza et al. 2018). Breast milk contains 6–20 g/L of nonconjugated carbohydrates which are known as human milk oligosaccharides (HMOs) (Ninonuevo and Lebrilla 2009; Bao et al. 2013; Auer et al. 2021). HMOs comprise >130 distinct structures and are the third most abundant component in breast milk after lactose and lipids (Bao et al. 2013; Nijman et al. 2018; Auer et al. 2021). HMOs can be categorized as neutral or acidic in nature depending on their monosaccharide composition (Plaza-Díaz et al. 2018). Neutral HMOs are further categorized into fucosylated and *N*-containing HMOs, the latter of which contains *N*-acetylglucosamine (GlcNAc) at the terminal positions (Plaza-Díaz et al. 2018). Acidic HMOs contain sialic acid (Neu5Ac) at one or both termini and represent 12%–14% of the total HMO content (Plaza-Díaz et al. 2018). HMOs help strengthen the immune system in infants, and they can prevent the adhesion of pathogens to epithelial cells, which blocks the initial step of infection (Ninonuevo and Lebrilla 2009; Remoroza et al. 2018). HMOs also serve as prebiotics that promote the growth of beneficial gut bacteria (Ninonuevo and Lebrilla 2009). Specific HMOs, including 2′-fucosyllactose (2′FL) and 3/6′-sialyllactose (3′SL; 6′SL), are beneficial to the brain development of infants (Ruhaak and Lebrilla 2012a; Berger et al. 2020; Gu et al. 2021).

HMOs can be seen with linear or branched structures of 3–10 monosaccharide constituents (Bao et al. 2013) and have a core structure at the reducing end commonly made with lactose (Galβ1-4Glc) or *N*-acetyllactosamine (Galβ1-4GlcNAc) (Remoroza et al. 2018; Auer et al. 2021). Elongation occurs through the addition of β-1,3- or β-1,6-linked lacto-*N*-biose (Galβ1-3GlcNAc, type I) or *N*-acetyllactosamine (Galβ1-4GlcNAc, type II) disaccharide component to the core structure. HMOs with linear and branched structures are named as "para"-HMOs and "iso"-HMOs, respectively (Bode 2012; Plaza-Díaz et al. 2018). Chain branching is mainly initiated with the introduction of disaccharide units to the main chain via β-1,6 linkages (Plaza-Díaz et al. 2018). The core and the elongated structures can be further modified with α-1,2-, α-1,3- or α-1,4-linked fucose (Fuc) or α-2,3- and/or α-2,6-linked Neu5Ac units, which results in a collection of both structural and linkage isomers (Bode 2012; Plaza-Díaz et al. 2018; Auer et al. 2021).

The biological activity and health benefits of HMOs depend on the details of the linkage patterns, the branching positions, and sites of modification, so a wide range of analytical techniques must usually be incorporated to fully characterize and quantify the different HMOs. Some of the key techniques that are widely used for HMOs analysis include size-exclusion chromatography (Marino et al. 2011; Grabarics et al. 2017), liquid chromatography (LC) (Austin and Bénet 2018; Remoroza et al. 2018), reversed-phase high-performance chromatography (Leo et al. 2010), high-pH anion-exchange chromatography (Gu et al. 2021), porous graphitized carbon (Hong et al. 2014; Gu et al. 2021), hydrophilic interaction liquid chromatography (HILIC) (Marino et al. 2011; Remoroza et al. 2018), capillary

Received: November 3, 2021. **Revised:** February 14, 2022. **Accepted:** February 23, 2022

electrophoresis (Bao and Newburg 2008; Galeotti et al. 2014), micellar electrokinetic chromatography (Porfirio et al. 2020), nuclear magnetic resonance (NMR) spectroscopy (Van Leeuwen et al. 2014), and mass spectrometry (MS) (Ninonuevo and Lebrilla 2009; Ruhaak and Lebrilla 2012b; Remoroza et al. 2018).

Offline and online MS profiling of HMOs have been considered as key techniques in characterizing HMOs, mainly due to the speed and ability to identify molecular masses and structural information (Adamson and Håkansson 2007). Offline-MS techniques, such as matrix-assisted laser desorption (MALDI)/ionization time-of-flight MS, are widely used for HMO characterization and are effective in distinguishing α-2,3 and α-2,6-sialylated isomers via postsource decay fragmentation (Von Seggern et al. 2003; Nie et al. 2012). Generally speaking, MALDI can tolerate high salt concentrations in the samples, but MALDI ionization tends to cause the unwanted loss of labile Neu5Ac groups, so it is sometimes limited in its application to HMOs (Von Seggern et al. 2003). These drawbacks can be overcome by performing suitable purification procedures and by using optimized matrices, which add complexity to the experimental workflow (Selman et al. 2012).

Electrospray ionization (ESI) and nano-ESI are useful in performing online-MS analysis for both derivatized and underivatized HMOs (De Leoz et al. 2019). Online separation techniques coupled with tandem MS (MS/MS) detection enable deeper insight into the structural characteristics of complex samples (Han and Costello 2011; Oursel et al. 2017). Glycosidic fragments (B/Y and C/Z) are produced when C-O glycosidic bonds are broken between 2 neighboring monosaccharide residues (Domon and Costello 1988). Cross-ring fragments (A/X) are produced when C-C or C-O bonds are broken within a monosaccharide ring (Domon and Costello 1988). Cross-ring cleavages tend to be less common because they require breaking 2 covalent bonds to be observed. Glycosidic fragments provide details about the composition and sequence of an oligosaccharide, but cross-ring fragments can provide details about the location of sugar modifications—like methylation, acetylation, and sulfation—and linkage positions between sugar residues (Domon and Costello 1988; Han and Costello 2011). Different MS/MS techniques have been involved in HMOs analysis and they have demonstrated characteristic features to each technique.

Collision-induced dissociation (CID) produces glycosidic cleavages and a few cross-ring cleavages of native HMOs (Mank et al. 2019). Even though CID can provide valuable diagnostic fragments (De Leoz et al. 2019; Mank et al. 2019), CID also enables rearrangements, consecutive, internal fragments and multiple neutral losses—such as H_2O and CO_2—which complicate the product ion spectra (Ernst et al. 1997; Schaller-Duke et al. 2018; De Leoz et al. 2019; Mank et al. 2019). CID with metalated HMOs provides more structurally informative fragments relative to their protonated equivalents (Adamson and Håkansson 2007; Han and Costello 2011; Schaller-Duke et al. 2018), and high-energy collision-induced dissociation can result in more cross-ring cleavages compared to conventional CID (Han and Costello 2011).

Electron-based ion activation methods, such as electron transfer dissociation (ETD) (Han and Costello 2011), negative electron transfer dissociation (NETD) (Wolff et al. 2010), electron capture dissociation (ECD) (Liu and Hakansson 2011), electron-induced dissociation (Wolff et al. 2008), electronic excitation dissociation (Tang et al. 2018), and electron detachment dissociation (EDD) (Adamson and Håkansson 2007), have all been applied in the MS/MS analysis of oligosaccharides. These techniques have generally reduced the loss of labile modifications relative to CID, and they generally provide better sequence coverage of oligosaccharides relative to CID (Schaller-Duke et al. 2018). Even though the electron-based ion-activation techniques are effective in the structural characterization of HMOs, most of these techniques are limited to Fourier-transform ion cyclotron resonance mass analyzers, whose expense limits widespread adoption (Adamson and Håkansson 2007; Han and Costello 2011).

Photon-based MS/MS dissociation methods, including infrared multiphoton dissociation (IRMPD) and ultraviolet photodissociation (UVPD), have created interest for the characterization of HMOs due to their ability to produce an array of informative cross-ring cleavages in a shorter timescale than most electron-based activation techniques (Ko and Brodbelt 2011). IRMPD provides similar results to CID and can be used as a complementary method to CID to gather structural details for HMOs (Schaller-Duke et al. 2018). UVPD is capable of producing diverse fragment ions, including cleavages within Neu5Ac, and the formation of UVPD-specific ^{4,5}X ions—even in the absence of derivatization—is highly beneficial in studies involving Neu5Ac (Devakumar et al. 2007; Wilson and Brodbelt 2008; Ko and Brodbelt 2011). Derivatization plays a significant role in UVPD analysis, which can directly affect the native structure analysis of oligosaccharides (Devakumar et al. 2007; Wilson and Brodbelt 2008; Ko and Brodbelt 2011; Ropartz et al. 2014).

Helium charge transfer dissociation (He–CTD) is an emerging ion-activation technique that shows promising results for oligosaccharides (Ropartz et al. 2016, 2017; Buck-Wiese et al. 2020; Pepi et al. 2020), peptides (Hoffmann and Jackson 2014), proteins (Li et al. 2018), and lipids (Li and Jackson 2017). He–CTD builds on the work of Schlathölter's group and Zubarev's group (Bari et al. 2010, 2011; Chingin et al. 2014) and uses a kiloelectronvolt beam of helium cations to ionize and fragment the precursor ions (Hoffmann and Jackson 2014; Sasiene, Mendis, Jackson et al. 2021). Like UVPD and some electron-based methods, He–CTD produces a variety of structurally informative A/X cross-ring cleavages (Ropartz et al. 2016, 2017; Buck-Wiese et al. 2020; Pepi et al. 2020; Sasiene, Mendis, Jackson et al. 2021; Sasiene, Mendis, Ropartz et al. 2021; Sasiene, Ropartz et al. 2021). Buck-Weise et al. showed that He–CTD can be used to determine the connectivity patterns of β-1,3- and β-1,4-linked native glycans, which is beneficial in linkage isomer differentiation (Buck-Wiese et al. 2020). More recently, ultrahigh performance liquid chromatography (UHPLC)–He–CTD–MS has been successfully used to analyze a range of complex oligosaccharides, including highly methylated pectins and highly sulfated carrageenan mixtures (Mendis et al. 2021a, 2021b). These studies have shown that UHPLC–He–CTD–MS is capable of providing a series of unambiguous fragments from both the reducing and nonreducing ends, which has aided in the identification of site-specific modifications and isomeric structures of oligosaccharides in complex mixtures (Mendis et al. 2021a, 2021b).

The current work employs UHPLC–He–CTD–MS for the structural determination of a series of neutral and acidic HMOs, including LNFP I, LNFP II, LSTa, LSTb, LSTc, and disialyllacto-*N*-tetraose (DSLNT). The structures are shown

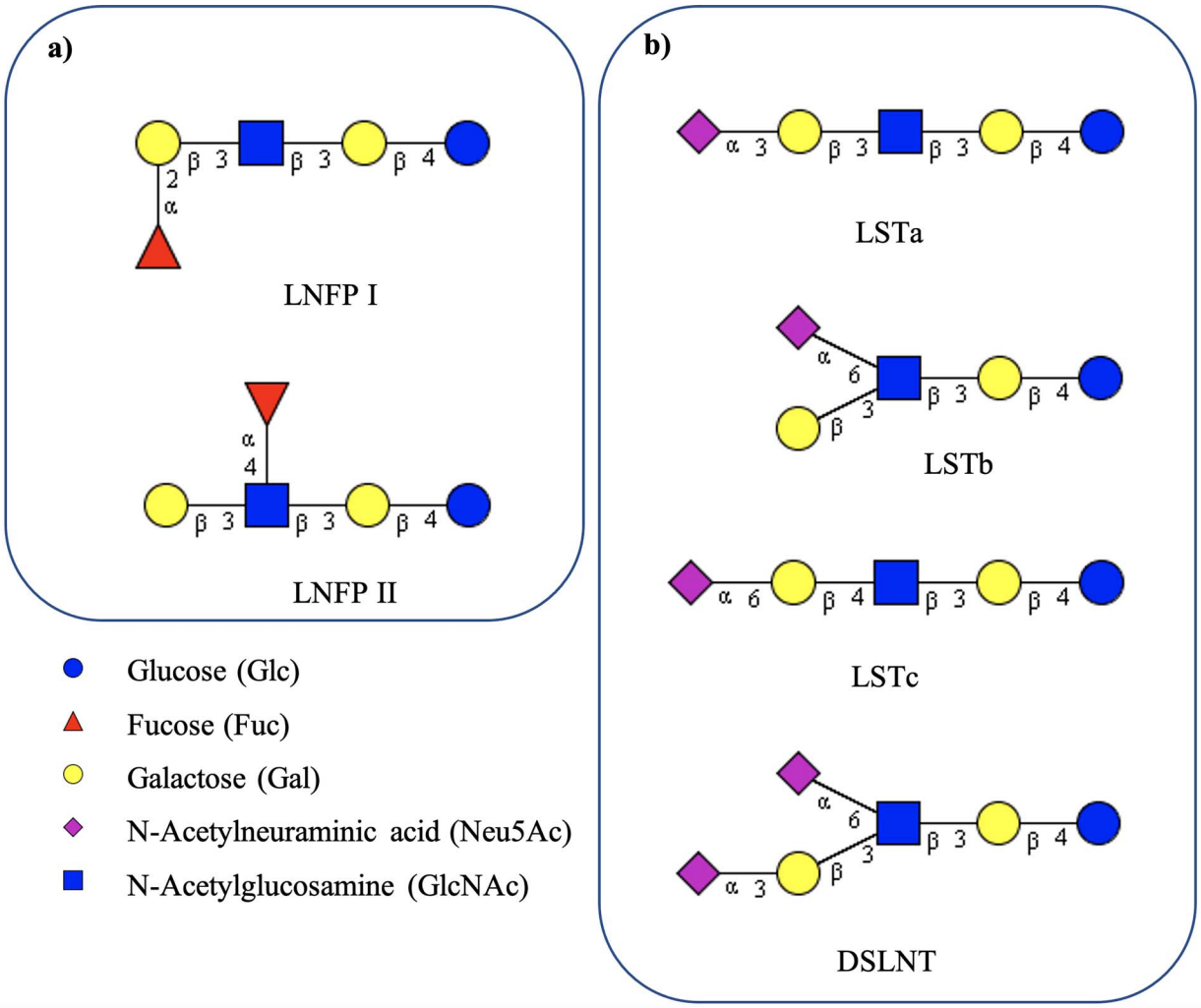

Fig. 1. A brief explanation of HMO compositions investigated in this work: a) neutral oligosaccharides and b) acidic oligosaccharides.

in Fig. 1. Results show that He–CTD produced more structurally informative cross-ring fragments than CID and that spectral acquisition rates are fast enough to handle complex mixtures of HMOs. The work demonstrates that He–CTD is a viable approach to high energy, radical-induced fragmentation of oligosaccharides, even when they are in the 1+ charge state and contain labile and acidic *N*-acetylneuraminic acid/sialic acid groups.

Results and discussion

First, we developed an optimized HILIC separation condition for a relatively simple synthetic mixture of HMOs. The mixture contained 2 neutral lacto-*N*-fucopentaoses (LNFP I and LNFP II), 3 acidic sialyllacto-*N*-tetraoses (LSTa, LSTb, and LSTc), and an acidic DSLNT. The standard mixture was selected because the components have been relatively well characterized by other novel methods of tandem MS and because they contain a variety of linkage patterns and modification sites of the labile sialic and fucose groups. Chromatographic separation was performed using the HILIC technique and the extracted ion chromatogram, as shown in Fig. 2, illustrates the elution profile of the HMO mixture.

Both the neutral and acidic HMOs show almost baseline separation under the HILIC conditions, which is consistent with the work of others (Marino et al. 2011; Grabarics et al. 2017; Remoroza et al. 2018). Neutral HMOs, such as LNFP I and II, elute first at 15.0 and 16.0 min (Marino et al. 2011; Remoroza et al. 2018). Neutral HMOs are nonsialylated compounds and are less polar than the acidic HMOs used in this study. Acidic HMOs, such as LSTa, LSTb, and LSTc, elute, respectively, at 16.2, 16.8, and 17.4 min. Acidic HMOs contain sialylated structures with additional carboxylic acid group(s), which display higher polarity compared to neutral oligosaccharides and elute later under HILIC conditions. Finally, DSLNT, which contains 2 Neu5Ac groups with a total of 2 carboxylic acid groups, is the largest in the size and has the highest polarity in the HMOs mixture; DSLNT therefore elutes last at 19.6 min.

After the HILIC separation, HMO compounds were analyzed with either He–CTD or CID. The observed product ions were annotated according to Domon and Costello, and the largest branch in the oligosaccharide structure represents by the symbol α (Domon and Costello 1988). The 2 neutral oligosaccharides, LNFP I and LNFP II, are structural isomers with different fucosylation positions (Pfenninger et al. 2002a, 2002b; Mank et al. 2019). For both LNFP I and LNFP II, the

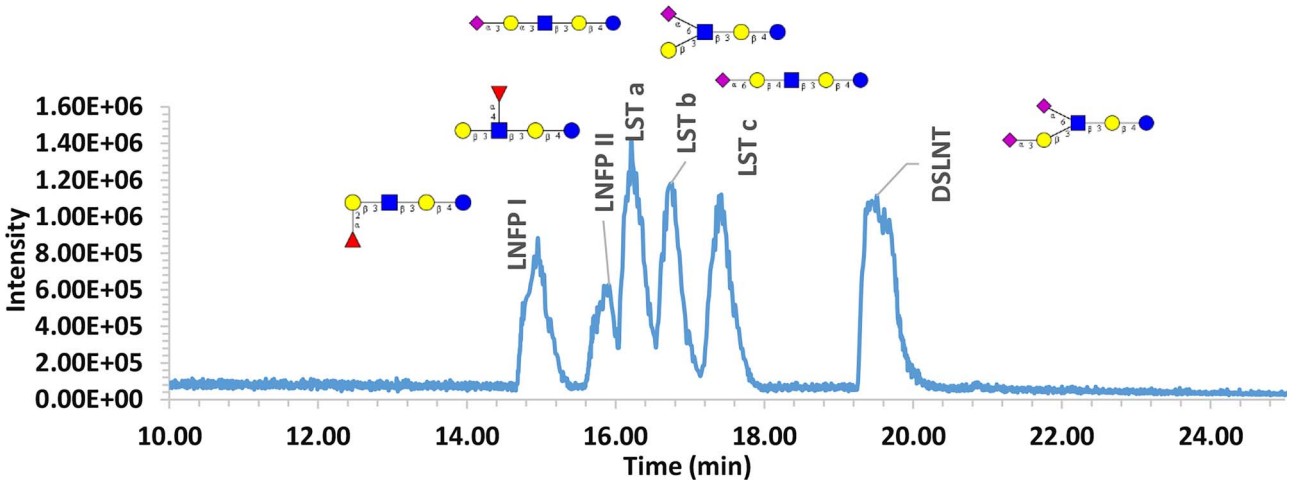

Fig. 2. Extracted ion chromatogram of HILIC separation of the complex mixture of milk oligosaccharides.

sodium adducted ion provided the most abundant precursor at mass-to-charge ratio (*m/z*) 876.3, so it was selected for MS/MS analysis. Sodium was not intentionally added to any of the mobile phases.

Figures 3a and 4a show the CID spectra for LNFP I and II, respectively. Figures 3b and 4b show the He–CTD spectra of the same precursors under otherwise-identical conditions. CID produced an array of glycosidic fragments in LNFP I, including many unambiguous B/Y and C/Z cleavages. The observed fragments are spread throughout the oligosaccharide backbone. Compared to LNFP I, LNFP II provided fewer unambiguous fragments with CID, and they are localized in between GlcNAc2 and Gal3 units. CID is able to produce diagnostic glycosidic fragment ions for each neutral HMO, including the C_2 fragment at *m/z* 349.0 (with LNFP I), and the C_2-$Z_{3\alpha}$ fragment at *m/z* 372.1 (with LNFP II), both of which comply with previous experiments using CID (Pfenninger et al. 2002a, 2002b; Mank et al. 2019). Both the diagnostic fragment ions provide valuable information on the composition of the nonreducing ends and are helpful in the preliminary differentiation of LNFP I and LNFP II (Mank et al. 2019). In addition, CID is able to produce unambiguous cross-ring fragments on the GlcNAc unit in both LNFP I and II ($^{2,4}X_2$ and $^{0,2}X_2$, respectively), but these fragments provide limited additional structural information.

In contrast to CID, He–CTD spectra for LNFP I and LNFP II, as shown in Figs. 3b and 4b, respectively, contain rich glycosidic and cross-ring fragments. The fragment ion maps inset in the figures shows that He–CTD produces several unambiguous fragments throughout the structures. Both LNFP I and II produced the diagnostic glycosidic products C_2 (*m/z* 349.1) and B_2-$Y_{3\alpha}$/C_2-$Z_{3\alpha}$ at (*m/z* 372.0), respectively, which help to distinguish each isomeric structure, as described by Mank et al. using CID. (Mank et al. 2019). He–CTD exhibits unambiguous cross-ring fragment ions, such as $^{1,5}A_n$, $^{1,5}X_n$, and $^{0,2}X_n$, with both LNFP I and II, and these informative fragments provide information on the location of the labile fucose unit and provide information on the linkage position between the monosaccharide units. The $^{1,5}A_n$, $^{1,5}X_n$, and $^{0,2}X_n$ fragments have been previously observed with UHPLC–He–CTD–MS for carrageenan oligosaccharides, and these cross-ring fragments were useful for localizing the labile sulfate modification positions on the oligosaccharide structures (Mendis et al. 2021a).

The presence of a Fuc1-Gal2-disaccharide unit at the nonreducing end in LNFP I is explained by the C_2 ion at *m/z* 349.1. The Y_4 and $^{1,5}X_4$ fragment ions also help narrow the fucose location to the terminal position. In LNFP II, the B_2-$Y_{3\alpha}$/C_2-$Z_{3\alpha}$ fragment at *m/z* 372.0 indicates the presence of a Gal-GlcNAc-Fuc unit at the nonreducing end, and the structural details obtained from the $^{1,3}A_2$, $^{0,2}X_2$ and $^{1,5}X_{3\alpha}$ fragment ions suggest that the terminal Gal1 is attached to GlcNAc2 via a 1,3-linkage. The $^{1,3}A_2$, $^{1,5}X_2$, and $^{1,5}X_{3\beta}$ fragment ions suggest that the branched fucose unit is attached to GlcNAc via a 1,4- or 1,6-linkage (Adamson and Håkansson 2007). The remaining product ions from LNFP I and II show that He–CTD is capable of preserving the labile fucose residue on a majority of the product ions and that He–CTD is able to evade the fucose migration that has plagued earlier CID studies (Wuhrer et al. 2006; Aldredge et al. 2013; Mank et al. 2019).

The acidic HMOs—LSTa, LSTb, and LSTc—provide a challenging family of sialylated isomers to resolve. The unambiguous fragment maps and spectra for each sialylated isomer with both CID and He–CTD are shown in Figs. 5–7 and Supplementary Figs. S1–S3. Among these oligosaccharides, LSTa and LSTc display linkage isomerism to each other, and LSTb shows structural isomerism to LSTa and LSTc (De Leoz et al. 2019). As observed in the unambiguous fragmentation maps for CID of three isomers in Figs. 5a–7a, glycosidic cleavages are dominant in CID and the cross-ring cleavages are infrequent and/or unhelpful. CID resulted in a series of unambiguous glycosidic cleavages from both the reducing and nonreducing termini with both LSTa and LSTc.

The CID fragments B_4 and Y_4 indicate the presence of terminal sialic acid and glucose units at nonreducing and reducing ends, respectively. Fragment pairs of B_2-Y_4, B_2-B_3, and B_3-B_4 provide the D-galactose-GlcNAc-D-galactose monosaccharide sequence in LSTa and LSTc. For LSTb, CID resulted in fewer unambiguous glycosidic cleavages, which makes the monosaccharide composition determination more difficult to assign. The glycosidic fragments C_2 and $Y_{3\alpha}$ (Supplementary Fig. S2a) indicate that the labile sialic acid unit tends to be absent with CID, and this neutral loss increases the uncertainty in the structural determination process (De Leoz et al. 2019).

In addition to the glycosidic cleavages, the CID spectra in Figs. 5a–7a demonstrate that there are several unambiguous

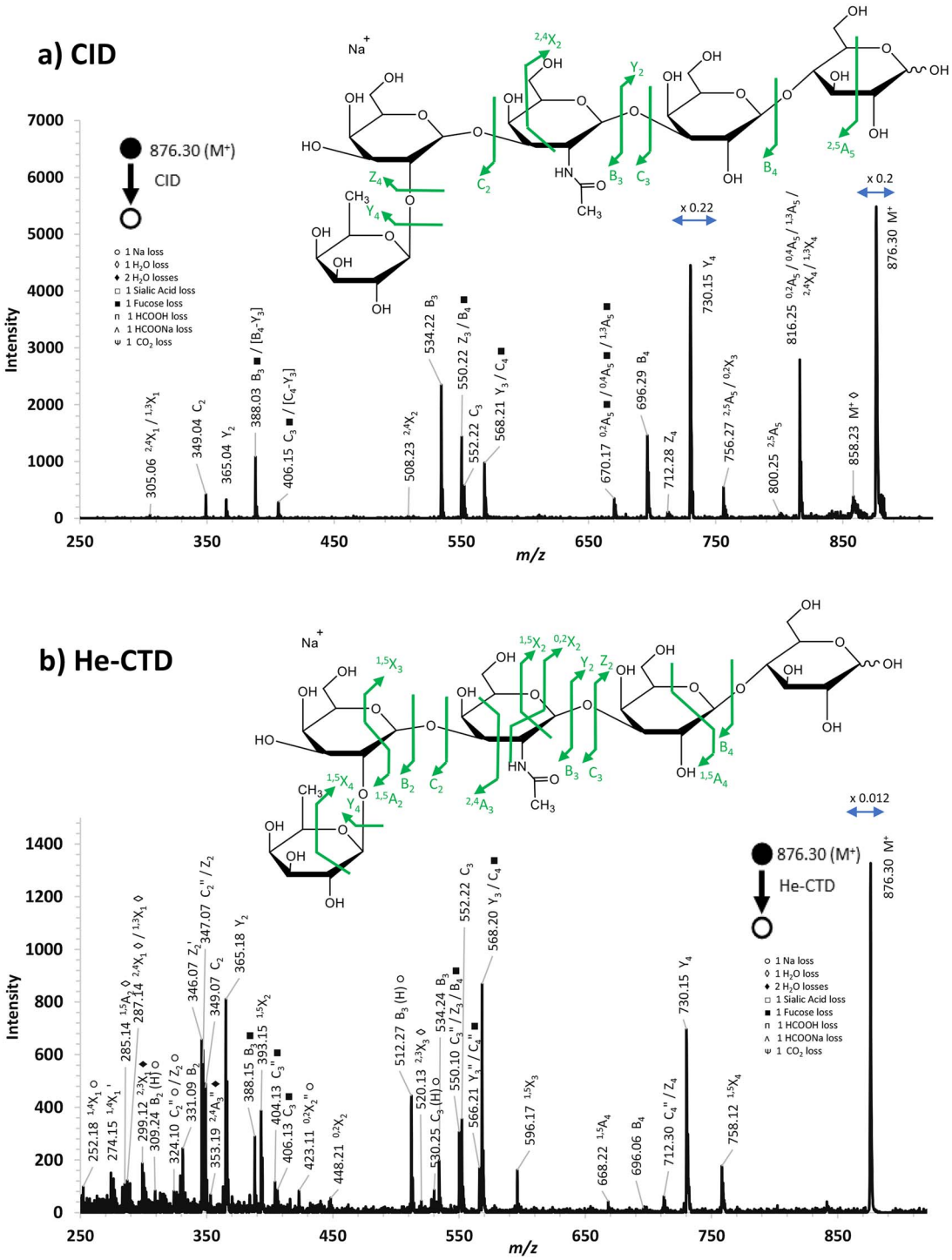

Fig. 3. HILIC–UHPLC–MS/MS spectra of LNFP I at 15.0 min collected in positive ion mode using a) CID and b) He–CTD. The insets show only the unambiguous annotated product ions.

cross-ring cleavages ($^{2,4}A_n$, $^{2,5}X_n$, and $^{0,2}X_n$) at the terminals of LSTa-c (Adamson and Håkansson 2007; De Leoz et al. 2019). The unambiguous $^{2,4}A_5$ and B_4 fragments, which are observed in LSTa and LSTc, provide details about the reducing end (De Leoz et al. 2019). For LSTb, the $^{0,4}A_2$ fragment at *m/z* 374.0 is the only unambiguous cross-ring fragment which is observed with CID. The presence of the $^{0,4}A_2$ cross-ring fragment ion is advantageous because it indicates the attachment of Neu5Ac to C-6 on the GlcNAc unit (Adamson and Håkansson 2007; Ko and Brodbelt 2011). In short, the level of detail provided by CID for these 3 isomers is not sufficient to differentiate them with confidence. Whereas differentiation can be accomplished by considering their elution times, the elution times of standards may not always be feasible when elucidating structures in natural samples.

The He–CTD MS/MS fragmentation maps for LSTa, LSTb, and LSTc are shown in Figs. 5b–7b, respectively. As shown in the fragmentation maps, He–CTD produces more glycosidic

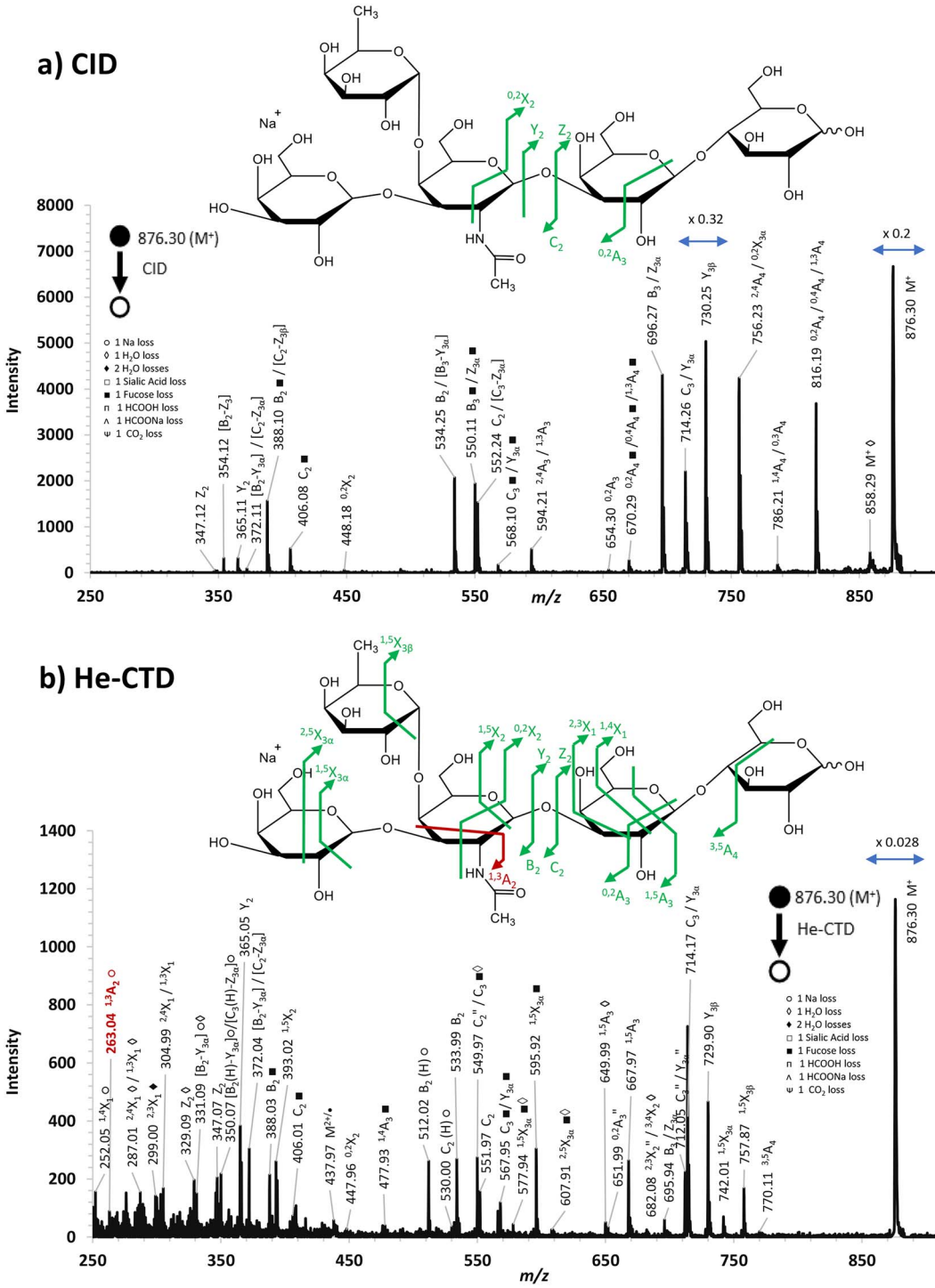

Fig. 4. HILIC–UHPLC–MS/MS spectra of LNFP II at 16.0 min collected in positive ion mode using a) CID and b) He–CTD. The insets show only the unambiguous annotated product ions.

fragments for all three HMOs, and the unambiguous glycosidic cleavages help to understand the monosaccharide composition of the oligosaccharides in a similar fashion in CID. In addition to the glycosidic fragments, He–CTD provides many cross-ring fragments, including $^{0,2}A_n$, $^{0,3}A_n$, $^{0,4}A_n$, $^{1,3}A_n$, $^{1,5}A_n$, $^{2,4}A_n$, $^{2,5}A_n$, $^{3,5}A_n$, $^{0,2}X_3$, $^{1,4}X_n$, $^{1,5}X_n$, and $^{2,5}X_n$. These structurally informative cross-ring fragments are beneficial in determining the linkage and branching patterns of the three isomers. As an example, He–CTD produced $^{2,4}A_3$, $^{1,3}A_3$, and $^{0,2}X_3$ product ions, and these ions are useful in identifying the 1,3-linkage between Gal2 and GlcNAc3. Similarly, the fragments $^{1,5}X_2$ and $^{2,5}A_3$ help localize the $-NHCOCH_3$ active group on GlcNAc in LSTa to the C2 position. Such details are not possible with CID because of the limited cross-ring cleavages (De Leoz et al. 2019). The linkage-related information has been previously observed with UHPLC–He–CTD–MS studies performed with highly methylated pectin and carrageenan oligosaccharides, which helps to identify the

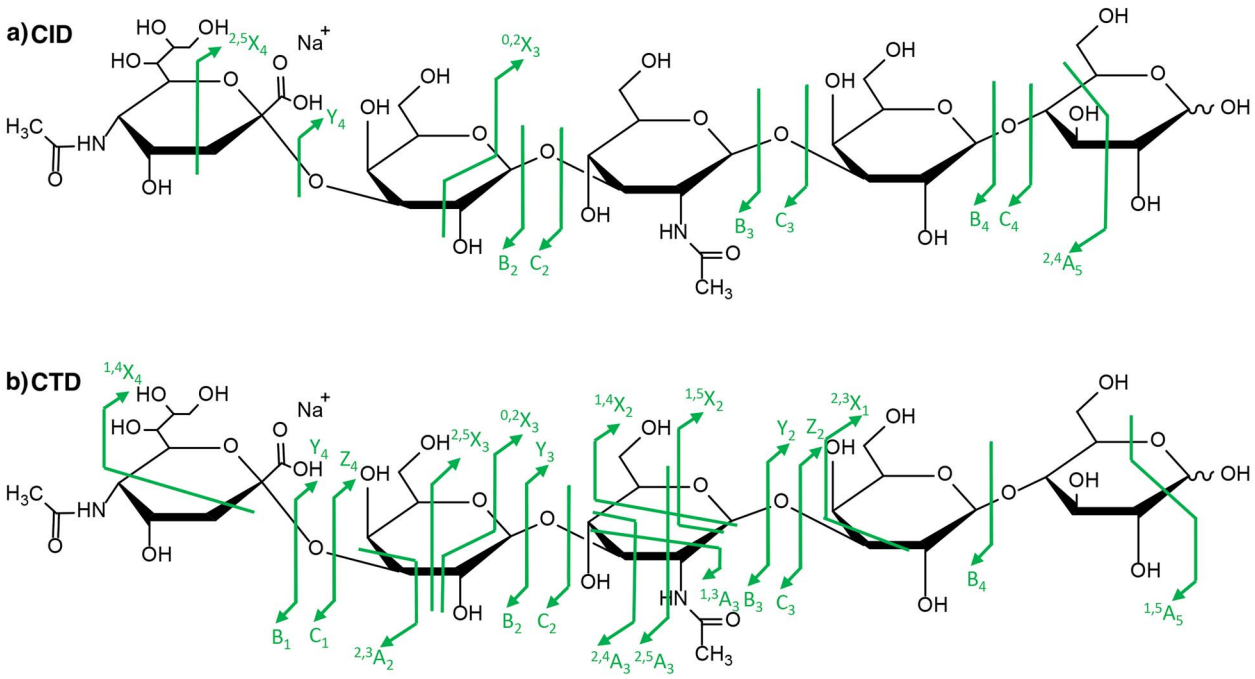

Fig. 5. HILIC–UHPLC–MS/MS product ion maps of LSTa at 16.2 min collected in positive ion mode using a) CID and b) He–CTD. The product maps show only the unambiguous annotated product ions.

1,4-linkage patterns between monosaccharide units and to localize the 6-O-methyl esterification and 4-O-sulfation sites on the oligosaccharides in the complex mixtures (Mendis et al. 2021a, 2021b).

The He–CTD product ion spectra for acidic HMOs also provide valuable information on the sialic acid linkage position, which is advantageous for isomer differentiation. The He–CTD spectrum for LSTa (Supplementary Fig. S1) indicates the presence of possible $^{1,3}A_2/^{2,4}A_2$ cross-ring ions at *m/z* 374.2, which have previously been observed with EDD for doubly deprotonated LSTa (Adamson and Håkansson 2007). The $^{1,3}A_2/^{2,4}A_2$ cross-ring ions suggest that Neu5Ac is attached to Gal2 at the C3 or C4 positions. In the He–CTD product ion spectrum for LSTb (Supplementary Fig. S2), the $^{0,3}A_2$ and $^{0,4}A_2$ fragments observed at *m/z* 374.2 and *m/z* 384.2, respectively, have been reported with ETD of Mg^{2+}-adducted LSTb, with UVPD of deprotonated LSTb, and with EDD of doubly deprotonated LSTb (Adamson and Håkansson 2007; Han and Costello 2011; Ko and Brodbelt 2011). These fragments provide details of the C6 linked Neu5Ac unit. For LSTb, He–CTD provides sufficient detail to localize the Neu5Ac attachment, and the presence of $^{1,5}X_{3\beta}$, $^{0,2}A_2$, and $^{0,3}A_2$ fragments confirm the presence of 1,3-linkage among the Gal-GlcNAc2 unit on the reducing terminus. When comparing the He–CTD spectra of LSTc with LSTb, LSTc follows a similar fragmentation pattern at the Neu5Ac location (Supplementary Fig. S3). The fragments $^{0,3}A_2$ and $^{0,4}A_2$ are also observed with LSTc, which again confirm the C6 position of the Neu5Ac residue to the Gal2 unit.

Some of these linkage-related fragments show product ions that are isobaric with different product ions from other isomers. Therefore, to be confident with the structural assignments, additional scrutiny is required. Table 1 shows a comparison of additional diagnostic peaks that correspond to each isomer. The peaks observed at *m/z* 415.1 $^{1,4}X_2$(H)-Na, *m/z* 528.2 Z_2(H)-Na/$^{0,2}A_3$-HCOONa, and *m/z* 546.2 Y_3(H)-Na are present above the minimal S/N level only in LSTa. Among those unique product ions, Y_3(H)-Na and $^{1,4}X_2$(H)-Na help to differentiate the unbranched structure of LSTa relative to LSTb. For LSTb, the peaks at *m/z* 517.2 B_2-Gal inform the presence of GlcNAc and Neu5Ac units in the nonreducing end, and the peak at *m/z* 292.1 ($B_{1\alpha}$) (Supplementary Fig. S2b) locates the Neu5Ac unit to the terminal position. Peaks observed at *m/z* 859.3 and *m/z* 399.1 are dominant only in LSTb, but further investigation needs to be performed with heavy ^{18}O labeling to break the ambiguity of the peak assignments. Labeling with heavy ^{18}O has been used successfully for He–CTD experiments for oligosaccharides in the past to differentiate ions originated from reducing and nonreducing termini (Ropartz et al. 2016). The dominant peak at *m/z* 384.2 $^{0,3}A_2''$-H_2O in LSTb and LSTc gives the information that LSTb and LSTc have a Neu5Ac attached at either C4 or C6 position, and this fragment is absent in LSTa. Peaks observed at *m/z* 454.0 B_2(H)-Na in both LSTa and LSTc indicate that LSTa and LSTc have unbranched nonreducing terminals compared to LSTb. With He–CTD, the D-galactose and GlcNAc residues at the nonreducing end in each isomer undergo multiple cross-ring cleavages. These extensive fragmentation patterns may be related to the elevated electron density in the acidic Neu5Ac residue and the increased propensity for ionization during cation–cation activation (Bari et al. 2010, 2011; Sasiene, Mendis, Jackson et al. 2021). Enhanced activation on the acidic, nonreducing terminus might also be related to the propensity for the adducting Na^+ ion to bind with Neu5Ac residue (Han and Costello 2011).

CID and He–CTD of disialylated branched oligosaccharide (DSLNT) are investigated, as shown in Supplementary

Fig. S4. In CID, fewer unambiguous glycosidic and cross-ring cleavages were observed, as expected. Similar to the monosialylated HMOs, the majority of the cross-ring cleavages—e.g. $^{0,2}X_{3\alpha}$ and $^{2,5}X_{3\alpha}$—occurred only on Gal2 units next to the Neu5Ac group. The presence of a $B_2/Y_{3\alpha}$ fragment provides informs us that one of the Neu5Ac groups is located at the nonreducing end. The presence of a B_3 ion and $B_2/Y_{3\alpha}$ fragment helps to locate the second Neu5Ac group on the GlcNAc3 unit. The lack of unambiguous cross-ring and glycosidic cleavages at the terminal sites

Table 1. Comparison of specific regions of He–CTD spectra to show structurally distinct product ions for the isomers LSTa, LSTb, and LSTc.

m/z	LSTa	LSTb	LSTc
384.2	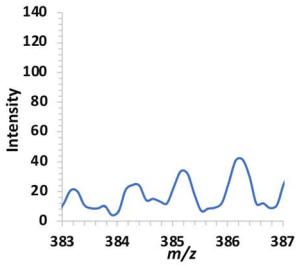	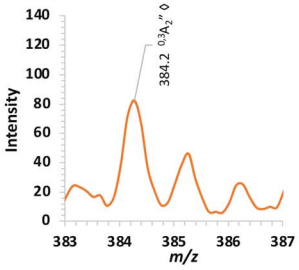	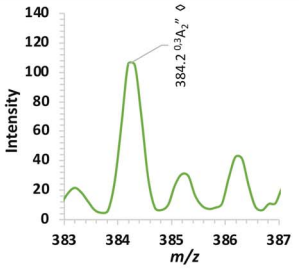
399.1	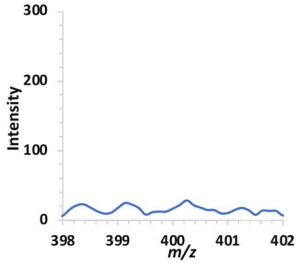	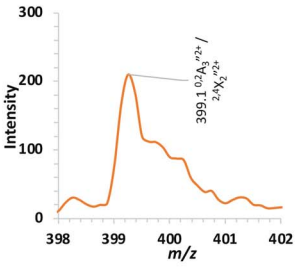	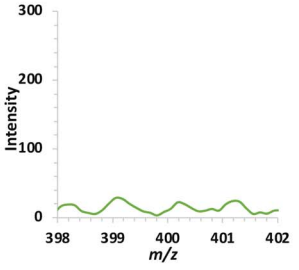
415.1	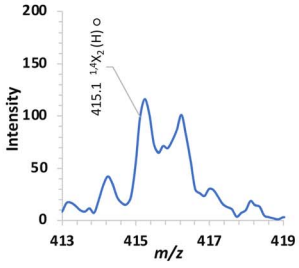	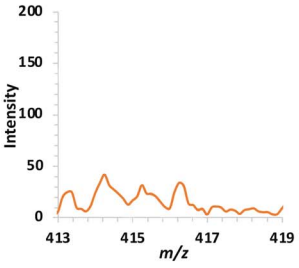	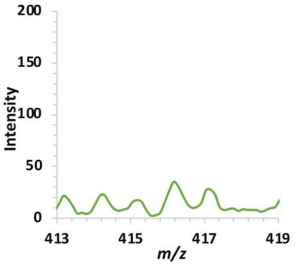
454.0	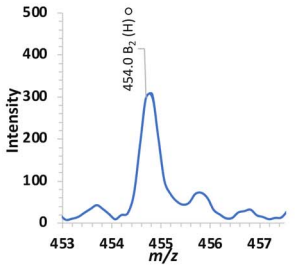	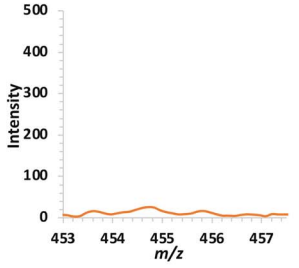	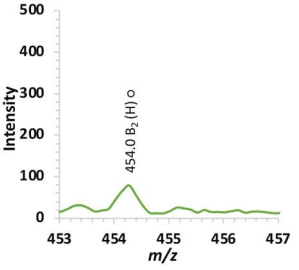
517.2	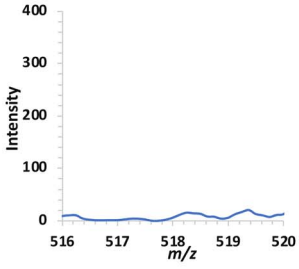	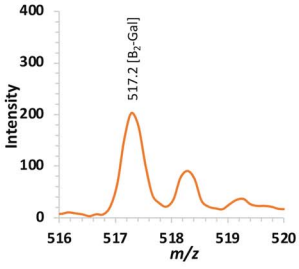	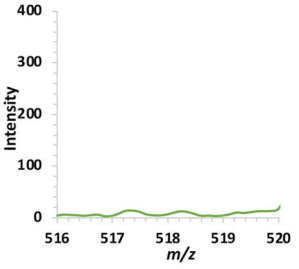

Continued

Table 1. Continued

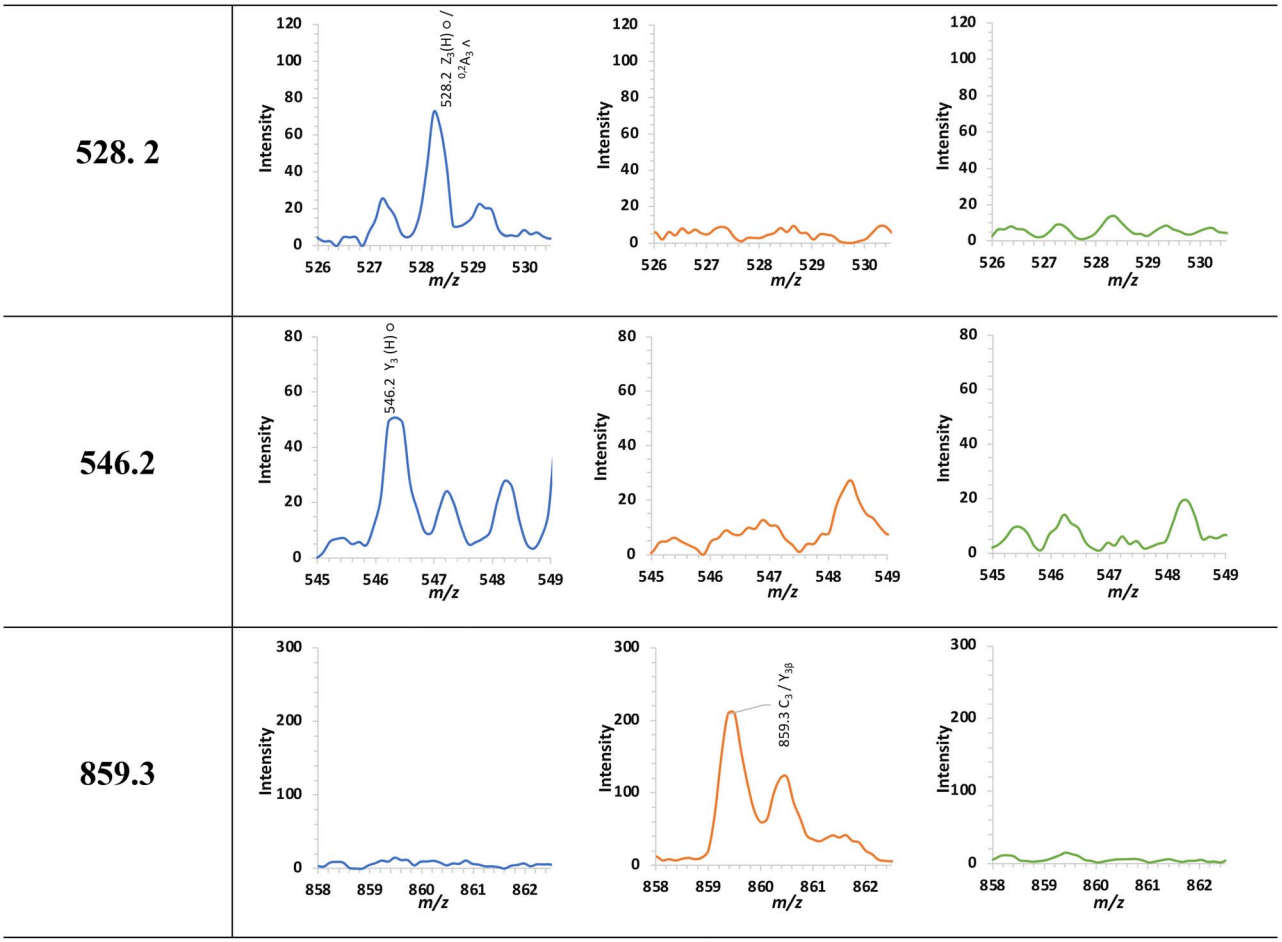

limits the structural information on the reducing and nonreducing ends.

In contrast to the CID results summarized above, He–CTD shows unambiguous glycosidic cleavages throughout the main branch, which helps to identify the monosaccharide sequence of the DSLNT. Unlike CID, He–CTD produces a majority of its unambiguous cross-ring cleavages on the GlcNAc at the center region. The unambiguous $^{2,4}A_3$ and $^{1,5}X_2$ cross-ring fragments enable the identification of the possible C3 or C6 attachment of the attached Neu5Ac group on the GlcNAc unit, which is a major advantage for He–CTD compared to CID. The $^{2,4}A$ and $^{1,5}X$ cross-ring cleavages have been previously reported with He–CTD for branched xyloglucans and, with the help of additional cross-ring fragments, such as $^{2,5}A$ and/or $^{2,5}X$, 1,4- and 1,6-linked branching patterns have been identified (Sasiene, Ropartz et al. 2021).

These results demonstrate the ability to perform HILIC–UHPLC–He–CTD–MS for effective analysis of a complex mixture of HMOs. He–CTD is capable of providing important cross-ring cleavages that help to differentiate linkage isomers and structural isomers in both neutral and acidic milk oligosaccharides. The beneficial cross-ring fragments observed with He–CTD show commonality with other radical and high energy activation techniques like ETD, EDD, and UVPD. Unlike some of the previously cited work, all the product ion spectra collected with He–CTD in this study are based on underivatized HMOs. He–CTD has a modest advantage of being applicable to the analysis of native HMOs. In addition, He–CTD is able to preserve the majority of the Neu5Ac and fucose residues. These findings give the impression that He–CTD is a valuable tool that can be used in the native structure analysis of oligosaccharides.

Materials and methods

Reagents and oligosaccharides

Ammonium formate was purchased from Oakwood Chemical (Estill, SC, USA). Formic acid (FA) and LC/MS grade acetonitrile (ACN) were purchased from ThermoFisher Scientific (Fair Lawn, NJ, USA). Ultrapure 18 MΩ water was obtained from a Milli-Q apparatus from Millipore (Burlington, MA, USA). Individual samples of sialylacto-*N*-tetraose a (LSTa), sialylacto-*N*-tetraose b (LSTb), sialylacto-*N*-tetraose c (LSTc), DSLNT, lacto-*N*-fucopentaose I (LNFP I), and lacto-*N*-fucopentaose II (LNFP II) were purchased from Biosynth Carbosynth (San Diego, CA, USA). The complex mixture of HMOs was prepared from the equimolar solutions of individual HMO samples.

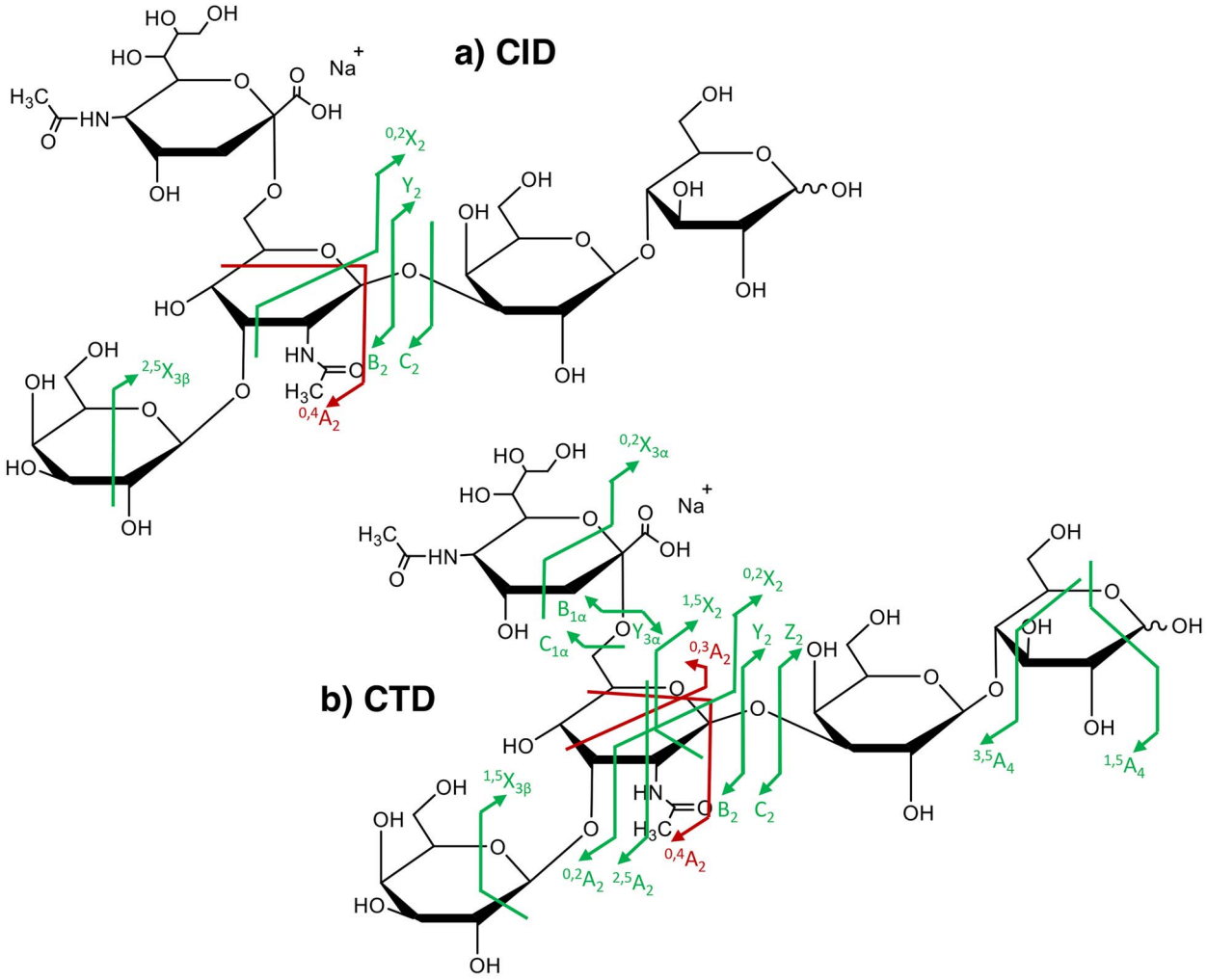

Fig. 6. HILIC–UHPLC–MS/MS product ion maps of LSTb at 16.8 min collected in positive ion mode using a) CID and b) He–CTD. The product maps show only the unambiguous annotated product ions.

HILIC separation

Chromatographic separation was performed on a Shimadzu Nexera X2 UHPLC system (Kyoto, Japan) using an Accucore 150-Amide-HILIC column (2.6 μm, 2.1 mm × 100 mm) from ThermoFisher Scientific. The composition of the 2 mobile phases was: (i) 99.9% ACN with 0.1% (v/v) FA and (ii) 10 mmol/L ammonium formate with 0.1% (v/v) FA. A binary gradient was used for the separation with a flow rate of 0.4 mL/min and column oven temperature of 50 °C. From 0–20 min, the composition was changed in a linear mode from 15% to 35% of mobile phase B. From 20–25 min, the gradient was changed in a linear mode from 35–75% mobile phase B. At 25 min, the column was re-equilibrated at 15% of mobile phase B for 5 min.

Online He–CTD

Online He–CTD was performed on a modified Bruker amaZon ETD quadrupole ion trap from Bruker Daltonics (Bremen, Germany), as described previously (Mendis et al. 2021a, 2021b). Briefly, a saddle field fast ion source from VSW/Atomtech (Macclesfield, UK) was fixed above a 3-mm hole in the ring electrode of the 3D ion trap and was connected to a variable leak valve (Model 203, Granville-Phillips) to control the flow of helium gas through the source. The flow of helium was indirectly measured from the ion gage in the main vacuum chamber and was kept at about ~1.2 × 10^{-5} mbar. The ion source was connected to an economical home-built system that employs a 10-kV Ultravolt HVA series high-voltage power supply (Advanced Energy, Denver, CO, USA). The +5.5 kV high voltage from the Ultravolt UHA was pulsed from ground to high with a rise time as fast as 150 ns by using a Behlke 101-03 switch (Behlke, Billerica, MA, USA). A TTL signal was taken from the MS^2 event of the Bruker amaZon from pin 28 of the auxiliary control port and was sent to an Agilent 33250A arbitrary function generator (AFG, Keysight Technologies, Santa Rosa, CA, USA) to provide an independently variable delay and pulse width. A DS1054 digital oscilloscope (Rigol, Beaverton, OR USA) compared the trigger waveform from the AFG with the scan function of the Bruker amaZon to ensure that the high-voltage pulses coincided with the desired storage period of the scan function. The saddle field fast ion source has an 85% conversion efficiency, so the 5.5 kV pulse provided helium cations with a kinetic energy of approximately 4.7 keV. The saddle field fast ion source pulse was matched with the fragmentation portion of the scan function of the instrument with the CID amplitude set to 0 V.

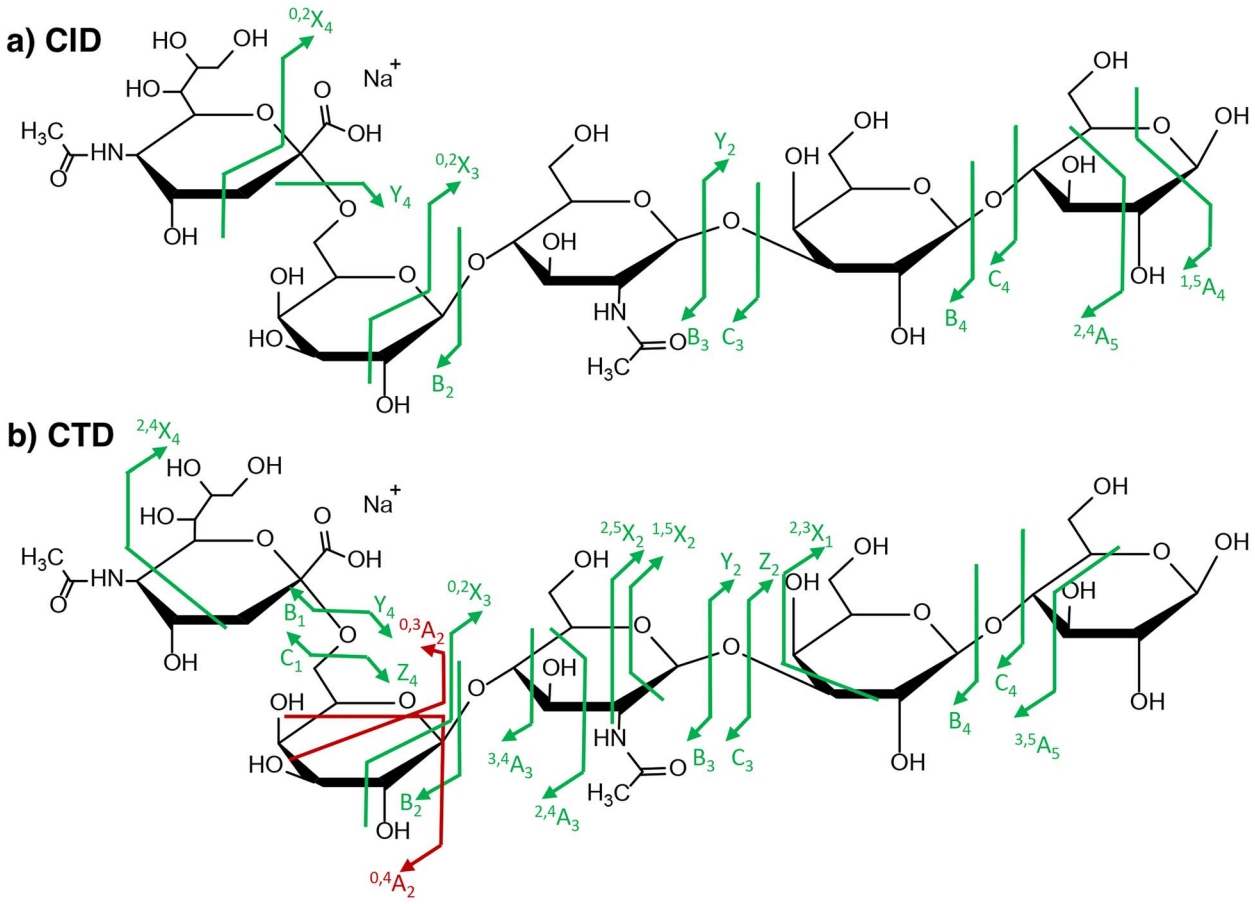

Fig. 7. HILIC–UHPLC–MS/MS product ion maps of LSTc at 17.4 min collected in positive ion mode using a) CID and b) He–CTD. The product maps show only the unambiguous annotated product ions.

UHPLC–HILIC–He–CTD–MS

The effluent from the UHPLC was connected to the standard Bruker Apollo ESI source (Billerica, MA). Capillary voltage and end cap voltage were set to +4,500 V and −700 V. Nebulizer pressure was set to 30 psi, the dry gas flow rate was set to 10 L/min and the dry temperature was at 340 °C. Experiments were conducted in the data-dependent acquisition (DDA) mode from *m/z* 250–1,500. The most abundant charge state of each analyte was chosen as the precursor ion with a window of 8 Da. The CID collision energy was set at 0 V when He–CTD was activated. The ion gun was pulsed on for 50 ms, and the MS^2 event, which includes the He–CTD activation time followed by a storage time, was set to 200 ms and a low mass cut-off of 27%. As a comparison, data of the same HMO mixture using the same UHPLC conditions were also collected using traditional CID-MS/MS on the same instrument with CID collision energy at 0.40 V and 50 ms activation time. For CID-MS/MS, smart fragmentation was on and set to 80%–120%.

Data analysis

Raw data were transformed in Bruker Compass DataAnalysis 4.0 SP4 software and were further processed using Microsoft Excel (Microsoft, Redmond, WA, USA). The peaks in the deconvoluted spectra were chosen manually based on their signal-to-noise ratio, isotope envelope distribution, and fragmentation patterns. Product ion assignments for CID and He–CTD were achieved using an in-house analysis of an HMO database and Glycoworkbench software. ChemDraw 19.1 (PerkinElmer, Walthman, MA, USA) was used for chemical structure illustrations.

Conclusions

The utility of UHPLC–He–CTD–MS has been demonstrated for the characterization of a complex mixture of neutral and acidic HMOs. Analytes in the mixture consisted of DP5 and DP6 linear and branched structures with labile Neu5Ac (sialic acid) and fucose residues. Our results demonstrate that He–CTD can perform effectively with the fast timescales and low sample loads required for HILIC–UHPLC separation and that it provides spectra with adequate signal-to-noise to determine the structural characteristics for HMOs. He–CTD product ion spectra contained a series of cross-ring and glycosidic cleavages, which allow an unambiguous identification of structural and linkage isomers in the HMOs mixture. The presence of $^{0,3}A_2$ and $^{0,4}A_2$ fragments in He–CTD are also observed with ETD, EDD, and UVPD and enable the differentiation of the α-2,3- versus α-2,6-linked Neu5Ac residues present among sialyllacto-*N*-tetraoses. The use of heavy ^{18}O labeling could resolve the identification of some ambiguous peak

assignments caused by the modest mass resolution of the 3D ion trap in this study. Finally, the results indicate that UHPLC–He–CTD–MS is a potential tool for the online characterization of biologically important oligosaccharides with diverse chemical properties. Expectations are that He–CTD will work equally well for the complex mixtures of *N*- and *O*-linked glycans.

Supplementary material

Supplementary material is available at *Glycobiology Journal* online.

Data Availability

Raw data available on demand from the corresponding author.

Acknowledgements

The opinions, findings and conclusions, or recommendations expressed in this publication are those of the author(s) and do not necessarily reflect the views of NSF or NIH. The authors thank William Feeney for providing the Accucore 150-Amide-HILIC column.

Funding

This work was supported by the National Science Foundation (CHE-1710376) and by the National Institute of Health (1R01GM114494–01).

Conflict of interest statement: None declared.

Abbreviations

ACN, acetonitrile; CID, collision-induced dissociation; DDA, data-dependent acquisition; DSLNT, disialyllacto-*N*-tetraose; ECD, electron capture dissociation; EDD, electron detachment dissociation; ESI, electrospray ionization; ETD, electron transfer dissociation; FA, formic acid; Fuc, fucose; GlcNAc, *N*-acetylglucosamine; He–CTD, helium charge transfer dissociation; He–CTD–MS, He–CTD mass spectrometry; HILIC, hydrophilic interaction liquid chromatography; HMOs, human milk oligosaccharides; IRMPD, infrared multiphoton dissociation; LC, liquid chromatography; LNFP, lacto-*N*-fucopentaose; *m/z*, mass-to-charge ratio; MALDI, matrix-assisted laser desorption/ionization; MS/MS, tandem mass spectrometry; NETD, negative electron transfer dissociation; Neu5Ac, sialic acid; NMR, nuclear magnetic resonance; UHPLC, ultrahigh performance liquid chromatography; UVPD, ultraviolet photodissociation.

References

Adamson JT, Håkansson K. Electron detachment dissociation of neutral and sialylated oligosaccharides. *J Am Soc Mass Spectrom*. 2007:**18**:2162–2172.

Aldredge DL, Geronimo MR, Hua S, Nwosu CC, Lebrilla CB, Barile D. Annotation and structural elucidation of bovine milk oligosaccharides and determination of novel fucosylated structures. *Glycobiology*. 2013:**23**:664–676.

Auer F, Jarvas G, Guttman A. Recent advances in the analysis of human milk oligosaccharides by liquid phase separation methods. *J Chromatogr B*. 2021:**1162**:122497.

Austin S, Bénet T. Quantitative determination of non-lactose milk oligosaccharides. *Anal Chim Acta*. 2018:**1010**:86–96.

Bao Y, Newburg DS. Capillary electrophoresis of acidic oligosaccharides from human milk. *Electrophoresis*. 2008:**29**:2508–2515.

Bao Y, Chen C, Newburg DS. Quantification of neutral human milk oligosaccharides by graphitic carbon high-performance liquid chromatography with tandem mass spectrometry. *Anal Biochem*. 2013:**433**:28–35.

Bari S, Hoekstra R, Schlatholter T. Peptide fragmentation by keV ion-induced dissociation. *Phys Chem Chem Phys*. 2010:**12**:3376–3632.

Bari S, Hoekstra R, Schlathölter T. Fast side-chain losses in keV ion-induced dissociation of protonated peptides. *Int J Mass Spectrom*. 2011:**299**:64–70.

Berger PK, Plows JF, Jones RB, Alderete TL, Yonemitsu C, Poulsen M, Ryoo JH, Peterson BS, Bode L, Goran MI. Human milk oligosaccharide 2′-fucosyllactose links feedings at 1 month to cognitive development at 24 months in infants of normal and overweight mothers. *PLoS One*. 2020:**15**:1–12.

Bode L. Human milk oligosaccharides: every baby needs a sugar mama. *Glycobiology*. 2012:**22**:1147–1162.

Buck-Wiese H, Fanuel M, Liebeke M, le Mai Hoang K, Pardo-Vargas A, Seeberger PH, Hehemann J, Rogniaux H, Jackson GP, Ropartz D. Discrimination of β-1,4- and β-1,3-linkages in native oligosaccharides via charge transfer dissociation mass spectrometry. *J Am Soc Mass Spectrom*. 2020:**31**:1249–1259.

Chingin K, Makarov A, Denisov E, Rebrov O, Zubarev RA. Fragmentation of positively-charged biological ions activated with a beam of high-energy cations. *Anal Chem*. 2014:**86**:372–379.

De Leoz MLA, Simón-Manso Y, Woods RJ, Stein SE. Cross-ring fragmentation patterns in the tandem mass spectra of underivatized sialylated oligosaccharides and their special suitability for spectrum library searching. *J Am Soc Mass Spectrom*. 2019:**30**:426–438.

Devakumar A, Mechref Y, Kang P, Novotny MV, Reilly JP. Laser-induced photofragmentation of neutral and acidic glycans inside an ion-trap mass spectrometer. *Rapid Commun Mass Spectrom*. 2007:**21**:1452–1460.

Domon B, Costello CE. A systematic nomenclature for carbohydrate fragmentations in FAB-MS/MS spectra of glycoconjugates. *Glycoconj J*. 1988:**5**:397–409.

Ernst B, Müller DR, Richter WJ. False sugar sequence ions in electrospray tandem mass spectrometry of underivatized sialyl-Lewis-type oligosaccharides. *Int J Mass Spectrom Ion Process*. 1997:**160**:283–290.

Galeotti F, Coppa GV, Zampini L, Maccari F, Galeazzi T, Padella L, Santoro L, Gabrielli O, Volpi N. Capillary electrophoresis separation of human milk neutral and acidic oligosaccharides derivatized with 2-aminoacridone. *Electrophoresis*. 2014:**35**:811–818.

Grabarics M, Csernák O, Balogh R, Béni S. Analytical characterization of human milk oligosaccharides—potential applications in pharmaceutical analysis. *J Pharm Biomed Anal*. 2017:**146**:168–178.

Gu F, ten Kate GA, Arts ICW, Penders J, Thijs C, Lindner C, Nauta A, van Leusen E, van Leeuwen SS, Schols HA. Combining HPAEC-PAD, PGC-LC–MS, and 1D1H NMR to investigate metabolic fates of human milk oligosaccharides in 1-month-old infants: a pilot study. *J Agric Food Chem*. 2021:**69**:6495–6509.

Han L, Costello CE. Electron transfer dissociation of milk oligosaccharides. *J Am Soc Mass Spectrom*. 2011:**22**:997–1013.

Hoffmann WD, Jackson GP. Charge transfer dissociation (CTD) mass spectrometry of peptide cations using kiloelectronvolt helium cations. *J Am Soc Mass Spectrom*. 2014:**25**:1939–1943.

Hong Q, Ruhaak LR, Totten SM, Smilowitz JT, German JB, Lebrilla CB. Label-free absolute quantitation of oligosaccharides using multiple reaction monitoring. *Anal Chem*. 2014:**86**:2640–2647.

Ko BJ, Brodbelt JS. 193 nm ultraviolet photodissociation of deprotonated sialylated oligosaccharides. *Anal Chem*. 2011:**83**:8192–8200.

Leo F, Asakuma S, Fukuda K, Senda A, Urashima T. Determination of sialyl and neutral oligosaccharide levels in transition and mature milks of Samoan women, using anthranilic derivatization followed by reverse phase high performance liquid chromatography. *Biosci Biotechnol Biochem*. 2010:**74**:298–303.

Li P, Jackson GP. Charge transfer dissociation of phosphocholines: gas-phase ion/ion reactions between helium cations and phospholipid cations. *J Mass Spectrom*. 2017:**52**:271–282.

Li P, Kreft I, Jackson GP. Top-down charge transfer dissociation (CTD) of gas-phase insulin: evidence of a one-step, two-electron oxidation mechanism. *J Am Soc Mass Spectrom*. 2018:**29**:284–296.

Liu H, Hakansson K. Electron capture dissociation of divalent metal-adducted sulfated oligosaccharides. *Int J Mass Spectrom*. 2011:**305**: 170–177.

Mank M, Welsch P, Heck AJR, Stahl B. Label-free targeted LC-ESI-MS2 analysis of human milk oligosaccharides (HMOS) and related human milk groups with enhanced structural selectivity. *Anal Bioanal Chem*. 2019:**411**:231–250.

Marino K, Lane JA, Abrahams JL, Struwe WB, Harvey DJ, Marotta M, Hickey RM, Rudd PM. Method for milk oligosaccharide profiling by 2-aminobenzamide labeling and hydrophilic interaction chromatography. *Glycobiology*. 2011:**21**:1317–1330.

Mendis PM, Sasiene ZJ, Ropartz D, Rogniaux H, Jackson GP. Ultrahigh-performance liquid chromatography charge transfer dissociation mass spectrometry (UHPLC-CTD-MS) as a tool for analyzing the structural heterogeneity in carrageenan oligosaccharides. *Anal Bioanal Chem*. 2021a:**414**:303–318.

Mendis PM, Sasiene ZJ, Ropartz D, Rogniaux H, Jackson GP. Structural characterization of isomeric oligogalacturonan mixtures using ultrahigh-performance liquid chromatography-charge transfer dissociation mass spectrometry. *Anal Chem*. 2021b:**93**:2838–2847.

Nie H, Li Y, Sun XL. Recent advances in sialic acid-focused glycomics. *J Proteome*. 2012:**75**:3098–3112.

Nijman RM, Liu Y, Bunyatratchata A, Smilowitz JT, Stahl B, Barile D. Characterization and quantification of oligosaccharides in human milk and infant formula. *J Agric Food Chem*. 2018:**66**:6851–6859.

Ninonuevo MR, Lebrilla CB. Mass spectrometric methods for analysis of oligosaccharides in human milk. *Nutr Rev*. 2009:**67**:S216–S226.

Oursel S, Cholet S, Junot C, Fenaille F. Comparative analysis of native and permethylated human milk oligosaccharides by liquid chromatography coupled to high resolution mass spectrometry. *J Chromatogr B Analyt Technol Biomed Life Sci*. 2017:**1071**: 49–57.

Pepi LE, Sasiene ZJ, Mendis PM, Jackson GP, Amster IJ. Structural characterization of sulfated glycosaminoglycans using charge-transfer dissociation. *J Am Soc Mass Spectrom*. 2020:**31**:2143–2153.

Pfenninger A, Karas M, Finke B, Stahl B. Structural analysis of underivatized neutral human milk oligosaccharides in the negative ion mode by nano-electrospray MSn (part 1: methodology). *J Am Soc Mass Spectrom*. 2002a:**13**:1331–1340.

Pfenninger A, Karas M, Finke B, Stahl B. Structural analysis of underivatized neutral human milk oligosaccharides in the negative ion mode by nano-electrospray MS n (part 2: application to isomeric mixtures). *J Am Soc Mass Spectrom*. 2002b:**13**:1341–1348.

Plaza-Díaz J, Fontana L, Gil A. Human milk oligosaccharides and immune system development. *Nutrients*. 2018:**10**:1038.

Porfirio S, Archer-Hartmann S, Brett Moreau G, Ramakrishnan G, Haque R, Kirkpatrick BD, Petri WA, Azadi P. New strategies for profiling and characterization of human milk oligosaccharides. *Glycobiology*. 2020:**30**:774–786.

Remoroza CA, Mak TD, De Leoz MLA, Mirokhin YA, Stein SE. Creating a mass spectral reference library for oligosaccharides in human milk. *Anal Chem*. 2018:**90**:8977–8988.

Ropartz D, Lemoine J, Giuliani A, Bittebière Y, Enjalbert Q, Antoine R, Dugourd P, Ralet MC, Rogniaux H. Deciphering the structure of isomeric oligosaccharides in a complex mixture by tandem mass spectrometry: photon activation with vacuum ultra-violet brings unique information and enables definitive structure assignment. *Anal Chim Acta*. 2014:**807**:84–95.

Ropartz D, Li P, Fanuel M, Giuliani A, Rogniaux H, Jackson GP. Charge transfer dissociation of complex oligosaccharides: comparison with collision-induced dissociation and extreme ultraviolet dissociative photoionization. *J Am Soc Mass Spectrom*. 2016:**27**: 1614–1619.

Ropartz D, Li P, Jackson GP, Rogniaux H. Negative polarity helium charge transfer dissociation tandem mass spectrometry: radical-initiated fragmentation of complex polysulfated anions. *Anal Chem*. 2017:**89**:3824–3828.

Ruhaak LR, Lebrilla CB. Analysis and role of oligosaccharides in milk. *BMB Rep*. 2012a:**45**:442–451.

Ruhaak LR, Lebrilla CB. Advances in analysis of human milk oligosaccharides. *Adv Nutr*. 2012b:**3**:406S–414S.

Sasiene ZJ, Mendis PM, Jackson GP. Quantitative assessment of six different reagent gases for charge transfer dissociation (CTD) of biological ions. *Int J Mass Spectrom*. 2021:**462**:116532.

Sasiene ZJ, Mendis PM, Ropartz D, Rogniaux H, Jackson GP. The influence of Na/H exchange on the charge transfer dissociation (CTD) spectra of mannuronic acid oligomers. *Int J Mass Spectrom*. 2021:**468**:116634.

Sasiene ZJ, Ropartz D, Rogniaux H, Jackson GP. Charge transfer dissociation of a branched glycan with alkali and alkaline earth metal adducts. *J Mass Spectrom*. 2021:**56**:e4774.

Schaller-Duke RM, Bogala MR, Cassady CJ. Electron transfer dissociation and collision-induced dissociation of underivatized metallated oligosaccharides. *J Am Soc Mass Spectrom*. 2018:**29**: 1021–1035.

Selman MHJ, Hoffmann M, Zauner G, McDonnell LA, Balog CIA, Rapp E, Deelder AM, Wuhrer M. MALDI-TOF-MS analysis of sialylated glycans and glycopeptides using 4-chloro-α-cyanocinnamic acid matrix. *Proteomics*. 2012:**12**:1337–1348.

Tang Y, Pu Y, Gao J, Hong P, Costello CE, Lin C. De novo glycan sequencing by electronic excitation dissociation and fixed-charge derivatization. *Anal Chem*. 2018:**90**:3793–3801.

Van Leeuwen SS, Schoemaker RJW, Gerwig GJ, Leusen-Van Kan EJM, Dijkhuizen L, Kamerling JP. Rapid milk group classification by 1H NMR analysis of Le and H epitopes in human milk oligosaccharide donor samples. *Glycobiology*. 2014:**24**:728–739.

Von Seggern CE, Zarek PE, Cotter RJ. Fragmentation of sialylated carbohydrates using infrared atmospheric pressure MALDI ion trap mass spectrometry from cation-doped liquid matrixes. *Anal Chem*. 2003:**75**:6523–6530.

Wilson JJ, Brodbelt JS. Ultraviolet photodissociation at 355 nm of fluorescently labeled oligosaccharides. *Anal Chem*. 2008:**80**: 5186–5196.

Wolff JJ, Leach FE III, Laremore TN, Kaplan DA, Easterling ML, Linhardt RJ, Amster IJ. Negative electron transfer dissociation of glycosaminoglycans. *Anal Chem*. 2010:**82**:3460–3466.

Wolff JJ, Laremore TN, Aslam H, Linhardt RJ, Amster IJ. Electron-induced dissociation of glycosaminoglycan tetrasaccharides. *J Am Soc Mass Spectrom*. 2008:**19**:1449–1458.

Wuhrer M, Koeleman CAM, Hokke CH, Deelder AM. Mass spectrometry of proton adducts of fucosylated N-glycans: fucose transfer between antennae gives rise to misleading fragments. *Rapid Commun Mass Spectrom*. 2006:**20**:1747–1754.